Hindawi
Shock and Vibration
Volume 2021, Article ID 8823150, 9 pages
https://doi.org/10.1155/2021/8823150

Research Article

Wet Modal Analyses of Various Length Coaxial Sump Pump Rotors with Acoustic-Solid Coupling

Guangjie Peng,[1,2] Zhuoran Zhang,[1] and Ling Bai[1]

[1]*National Research Center of Pumps, Jiangsu University, Zhenjiang, Jiangsu 212013, China*
[2]*State Key Laboratory of Hydroscience and Engineering, Beijing 100084, China*

Correspondence should be addressed to Ling Bai; lingbai@ujs.edu.cn

Received 18 September 2020; Revised 16 November 2020; Accepted 6 February 2021; Published 15 February 2021

Academic Editor: Roman Gabl

The dynamic characteristics of the rotor components were determined using a first-order modal model of the rotor components for various sump pump shaft lengths for actual working environments. By employing ANSYS-Workbench software, this paper uses a fluid-solid coupling analysis to calculate the reaction forces of the fluid on the rotor with results, which is then used in dry and wet modal analyses of the rotor parts to calculate the vibration modal characteristics with and without prestresses. The differences between the wet and dry modal characteristics were compared and investigated by ANSYS. The results show that increasing the sump pump shaft length reduces the first-order natural frequency of the prestressed rotor components. The structure also experiences stress stiffening, which is more obvious in the high-order modes. The natural frequency of the rotor in the wet mode is about 16% less than that in the dry mode for the various shaft lengths due to the added mass of the water on the surface which reduces the natural frequency. In the wet modal analysis, when the structure is in a different fluid medium, the influence of its modal distribution will also change, this is because the additional mass produced by the fluid medium of different density on the structure surface is different. Thus, the wet modal analysis of the rotor is important for more accurate dynamic analyses.

1. Introduction

A sump pump is a vertical pump that all the flow components, such as the impeller and the pump body, are immersed in the fluid when connected to the motor [1]. The motor is fastened to the motor base and drives the rotor through a coupling [2]. There are many kinds of sump pumps. Traditional sump pumps are used to transport corrosive materials such as strong acids, alkalis, salts [3], and strong oxidants [4] at various concentrations. New sump pumps are used to transport flammable and explosive materials. The liquid level in the pump can be changed by changing the shaft length for various applications.

The working environment of sump pumps is complicated, and it is often affected by dynamic loads such as wave currents and shock vibrations [5]. The vibration of the structure not only affects the working stability but also affects the fatigue life [6]. Therefore, understanding the natural frequency and critical speed of the structure can provide a certain basis for preventing the structure from resonance damage and vibration fatigue, evaluating the dynamic characteristics of the structure and optimizing the structure [7, 8]. Rotating machinery often undergoes lateral bending vibration due to the eccentricity of the elastic rotor of the rotating shaft during operation. When the speed increases to a certain value, the amplitude will suddenly increase and the vibration will be extremely intense. When the speed exceeds this certain value, the amplitude will quickly decrease. This specific value is called the critical speed of the rotor. Safe operation of the sump pump requires that the rotor speed avoids the critical speed, so the critical speed should not be within 20% of the operating speed [9]. Vibration modal analyses are used to analyze the complex dynamic characteristics. Therefore, good dynamic characteristic analyses require accurate modal analyses for the actual operating conditions.

The literature has numerous studies on the internal flow characteristics and structural optimization of sump pumps [10, 11]. However, there are few modal analyses of sump pump

rotor components. The sump pump rotor components are subjected to axial and radial forces during operation, including the fluid force, gravity, and centrifugal forces. The fluid force then leads to stress stiffening which changes the rotor modal distribution [12, 13]. In addition, when the impeller rotates in the fluid, the additional mass produced by the fluid on the structure varies as the rotor rotates which also affects the modal characteristics [14–16]. Therefore, sump pump designs must include modal analyses of the rotor components.

In this study, the reaction force of the fluid on the impeller of sump slurry pump was calculated using a coupled fluid-solid analysis [17, 18]. The prestresses due to these forces were then used in the "dry" and "wet" modal analyses of the sump pump rotor [19] to determine the natural frequency and critical speed of the rotor. The natural frequency and critical speed of the sump pump rotor were then calculated for various shaft lengths. Comparisons with existing manufacturer data verified the accuracy of the simulation results. These results provide a reference for analyses of the structural dynamic characteristics of sump pumps to improve the structural designs.

2. Modal Analysis Theory

The general dynamics equation describing discrete vibrations with N degrees of freedom in the physical coordinate system [19] is

$$[M]\{u\} + [C]\{u\} + [k]\{u\} = \{F(t)\}, \tag{1}$$

where $[M]$ is the mass matrix (symmetric and positive definite), $[C]$ is the damping matrix, $[K]$ is the stiffness matrix (symmetric and positive definite or semipositive definite), and $\{F(t)\}$ is the N-dimensional excitation force vector. The excitation forces in this study include the fluid force, gravity, and centrifugal force.

Assuming that the initial system state is stationary, the Laplace transform of equation (1) is

$$\left([M]s^2 + [C]s + [K]\right)\{X(s)\} = [Z(s)]\{X(s)\} = \{F(s)\}, \tag{2}$$

where [Z (s)] is

$$[Z(s)] = \left([M]s^2 + [C]s + [K]\right), \tag{3}$$

which reflects the dynamic characteristics of the system and is called the system dynamics matrix or the generalized impedance matrix.

In equation (3), $s = j\omega$ and the impedance matrix is

$$[Z(\omega)] = \left([K] - \omega^2[M]\right) + j\omega[C]. \tag{4}$$

The frequency response function matrix in terms of the modal parameters is then

$$[H(\omega)] = [Z(\omega)]^{-1} = [\phi]\left[Z_r\right]^{-1}[\phi]^T = \sum_{r=1}^{N} \frac{\{\phi_r\}\{\phi_r\}^T}{m_r\left[\left(\omega_r^2 - \omega^2\right) + 2j\xi_r\omega_r\omega\right]}. \tag{5}$$

The elements of $[H(\omega)]$ in row i and column j of the matrix are

$$H_{ij}(\omega) = \sum_{r=1}^{N} \frac{\phi_{ri}\phi_{rj}}{m_r\left[\left(\omega_r^2 - \omega^2\right) + 2j\xi_r\omega_r\omega\right]}, \tag{6}$$

where $\omega_r^2 = (k_r/m_r)$ is the frequency of mode r, $\xi_r = (c_r/2m_r\omega_r)$ is the damping ratio of mode r, and $\{\phi_r\}$ is the mode shape of mode r.

The frequency response of an N degree-of-freedom system is then equal to the linear combination of the frequency responses of N single-degree-of-freedom systems. All the modal parameters can then be determined from only one column or one row of the frequency response function matrix.

3. Modeling, Meshing, and Boundary Conditions

3.1. 3D Model and Mesh. Figure 1 shows the rotor components of the 100SP sump pump. The sump pump rotor consists of an impeller, a pump shaft, and two bearings. The impeller is an open impeller. Table 1 shows the main parameters of the sump pump. The pump assembly drawing is shown in Figure 2 where length $A = D + 529$, length $B = \mathrm{D} - 348$, and D is the pump installation elevation which was varied to vary the pump shaft length ($D = 1500$ for the standard design pump). Table 2 lists the pump shaft lengths for various D. The sump pump flow region included the inlet extension, impeller, volute, and outlet extension. The flow region was modeled in a 3D model, as shown in Figure 3. The fluid domain model uses ANSYS-ICEM for unstructured meshing, and the mesh quality is above 0.3. The solid domain model is adaptive tetrahedral meshing, and the average mesh quality is above 0.7, as shown in Figure 4. In order to study whether the number of grids will affect the calculation results, it is also necessary to verify the grid independence. In this paper, 4 sets of different numbers of sump pump fluid domain model grids are selected, and a set of reasonable number of grids is selected through calculation and comparison of the head changes at $Q = 216\ \mathrm{m}^3/\mathrm{h}$. It can be seen from Table 3 that when the number of selected 4 sets of grids is very different, the fluctuation range of the calculated head is within 1.5%. Starting from the selected second set of grids, the calculated head value has become flat, so the second set of grids is considered appropriate. The fluid domain had 2,400,584 elements while the solid domain had 273,376 elements.

The impeller and pump shaft material properties are listed in Table 4.

3.2. Boundary Conditions. The pump components modal distribution was calculated in the presence of prestresses due to the fluid forces. This paper takes the clean water as the research medium, and the density and sound velocity properties of the required water will be defined when the acoustic-structure coupling method is used for the wet modal analysis later. The flow field in the submerged pump is unsteady, so the flow calculations should be unsteady. However, the natural frequencies for steady and unsteady flow conditions are known to be very similar [20], so a steady

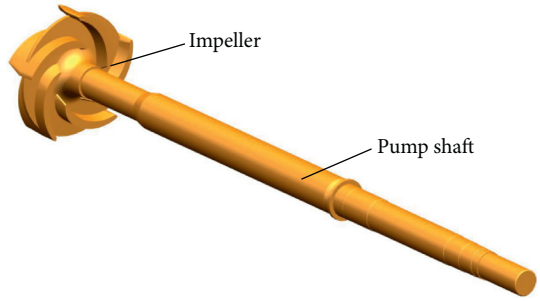

Figure 1: Solid model of sump pump rotor.

Table 1: Sump pump design parameters.

Flow rate Q ($m^3 \cdot h^{-1}$)	Head H (m)	Diameter D_2 (mm)	Blade number z	Speed n ($r \cdot min^{-1}$)	Outlet D_d (mm)	Maximum power P (kW)
216	32	370	5	1000	100	75

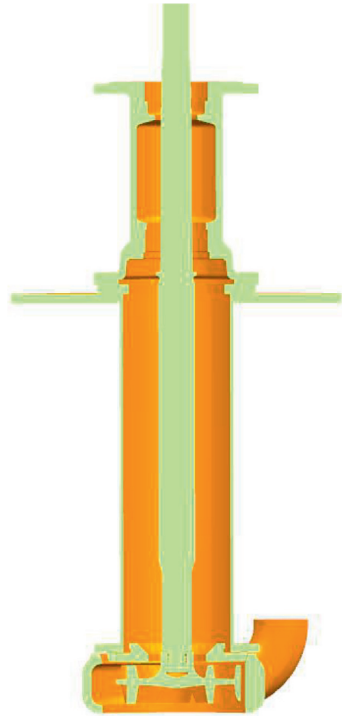

Figure 2: Sump pump assembly drawing.

Table 2: Pump shaft lengths for various D.

D (mm)	900	1200	1500	1800	2000	2400	2700	3000
A (mm)	1429	1729	2029	2329	2529	2929	3229	3529
B (mm)	552	852	1152	1452	1652	2052	2352	2652

flow field was used here for the calculations. The flow calculations assumed that the fluid was a steady incompressible flow with the standard $k - \varepsilon$ turbulence model [21]. The inlet was set as a total pressure inlet, the outlet was set as a mass flow outlet, and the walls were set as nonslip walls. In the solid domain, the submerged pump was assumed to have rigidly supported rolling bearings constrained by a cylindrical surface, so all the radial degrees of freedom were fixed. The shaft end and the coupling were connected with fixed restraints. The pump shaft and the impeller were connected by a key and a contact surface.

4. Results and Analysis

4.1. Experimental Validation. Before the modal analysis, the full flow field in the sump pump was predicted for various working conditions to obtain the flow-head curve for the sump pump to compare with manufacturer data, as shown

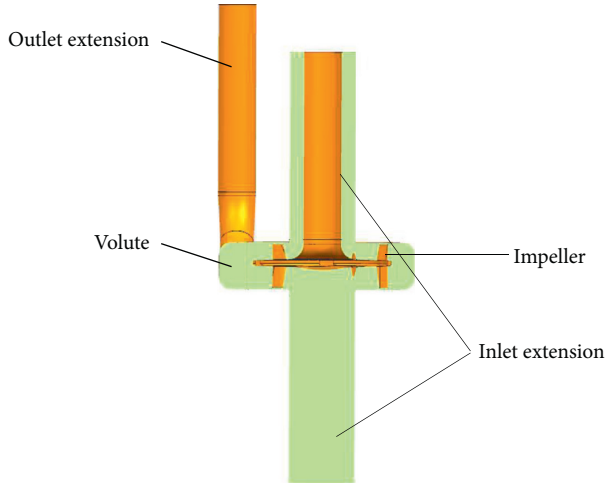

Figure 3: Sump pump fluid domain.

Figure 4: Solid domain mesh.

Table 3: Predicted sump pump performance under different grid numbers.

Number of grids	Head (m)
1264983	31.8
2400584	31.5
3881091	31.3
5532742	31.4

Table 4: Material properties.

Rotor part	Material	Density ρ (kg$*$m^{-3})	Elastic modulus E (GPa)	Poisson's ratio μ
Pump shaft	40Cr	7870	211	0.3
Impeller	#45 steel	7850	205	0.25

in Figure 5. The manufacturer data shown in Table 5 came from the characteristic curve released by Warman International [22].

The predicted heads agree well with the manufacturer data, as shown in Figure 5 with the same trends which shows that the steady flow field predictions are quite accurate. The mode analysis used the flow field at the rated flow of $Q = 216\ \mathrm{m}^3/\mathrm{h}$.

4.2. Dry Mode Analyses of Rotors with Various Shaft Lengths

4.2.1. Dry Mode Analysis without the Prestresses. The dry modal analysis without prestresses is a modal analysis in a vacuum without other factors to determine the natural frequency of the rotor system. The system constraints include the fixed constraint where the top of the rotor is connected to the coupling and the cylindrical constraint at the bearing, as shown in Figure 6 for a standard pump as an example, where A is the rolling bearing support, B is the cylindrical surface constraint, and C is the consolidation surface support.

The dry modal analysis was applied to the standard pump rotor along with various other shaft lengths without the prestresses and with the same constraint conditions to calculate the first-order natural frequencies listed in Table 6.

Without the prestress, the first-order natural frequency of the sump pump rotor gradually decreases with increasing shaft length with the rate of change gradually decreasing. With the fixed support conditions, increasing the shaft length increases the shaft support span which reduces the strength and the natural frequency of the rotor.

4.2.2. Dry Modal Analysis with the Prestresses. The dry modal analysis with the prestresses is a modal analysis with the rotor operating in a vacuum. The prestresses in the rotor components during operation include the gravitational force on the rotor itself, the centrifugal force generated by the

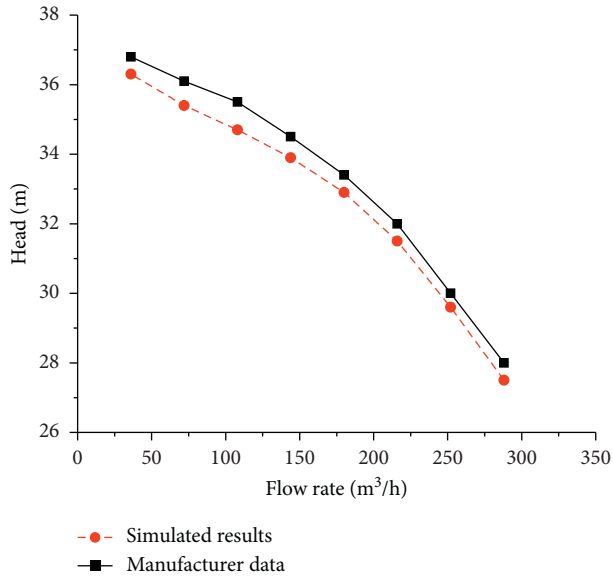

Figure 5: Predicted and measured [22] pump curves.

Table 5: Measured flow characteristics.

Flow rate, Q (m^3*h^{-1})	36	72	108	144	180	216	252	288
Head (manufacturer data), H (m)	36.8	36.1	25.5	34.5	33.4	32	30	28
Head (simulated results), H (m)	36.3	35.4	34.7	33.9	32.9	31.5	29.6	27.5

Figure 6: Constraints on the rotor.

Table 6: First natural frequencies for the various rotor lengths without prestresses.

D (mm)	900	1200	1500	1800	2000	2400	2700	3000
First natural frequency f (Hz)	54.513	32.717	22.024	16.143	13.220	9.320	7.549	6.218

rotation, and the force of the water on the impeller. The system constraints are the same as without the prestresses. Since the sump pump is vertical, gravity acts directly along the pump axis. The centrifugal force is related to the rotational speed of the rotor and the fluid force is loaded on the impeller blades and hub. The specific results are shown in Figure 7 which shows that the maximum fluid force on the impeller appears at the blade outlet with the minimum fluid force at the blade root. In the figure, the imported pressure represents the fluid force loaded on the blade while imported pressure 2 and imported pressure 3 represent the fluid forces loaded on the impeller hub.

The dry modal analysis of the pumps with various shaft lengths with the prestresses gave the first natural frequencies of the rotors listed in Table 7. Figure 8 shows that the rotor natural frequencies with and without the prestresses are basically the same. The first-order critical speed again decreases with increasing shaft length, while the first-order natural frequencies of the rotor components are slightly higher than without the prestresses, which shows that the prestresses make the pump rotor components and the structure more rigid. This stiffening is more obvious for the higher-order modal natural frequencies for $D = 1500$, as shown in Figure 9. The natural frequency of the third-order mode increases the most, reaching 16.82 Hz, while the natural frequencies of the other modes all increase more than the natural frequency of the first-order mode, indicating increased stress rigidity at higher-order modes. The higher-order natural frequencies for other D also showed this phenomenon.

4.3. Wet Modes of Rotors with Various Shaft Lengths with Prestresses. The wet modal analysis with prestresses models the rotor running in a fluid. The modal analysis in the "wet" state is closest to the actual rotor operation. This not only considers the effect of the prestresses on the rotor but also considers the additional mass due to the fluid on the surfaces

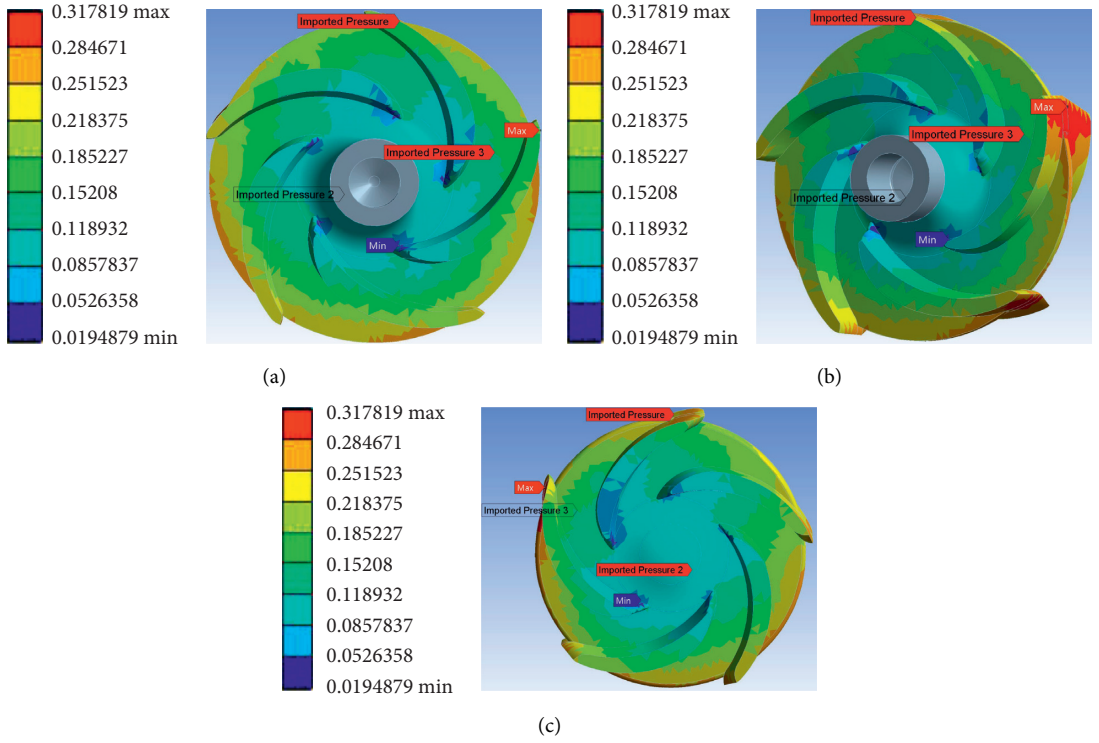

Figure 7: Flow forces on the impeller. (a) View from the front, (b) view from the side, and (c) view from the back.

Table 7: First natural frequencies of the various length rotors with the prestresses.

D (mm)	900	1200	1500	1800	2000	2400	2700	3000
First natural frequency (with prestress) f (Hz)	57.444	34.879	23.331	17.115	13.975	9.905	7.989	6.578
First natural frequency (without prestress) f (Hz)	54.513	32.717	22.024	16.143	13.220	9.320	7.549	6.218

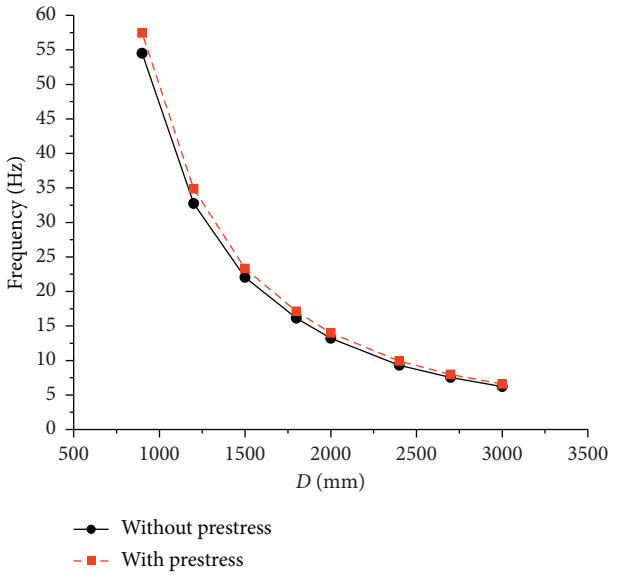

Figure 8: Influence of the prestresses on the first natural frequency.

when the rotor is running. In the dry modal analysis, the vacuum had negligible influence on the vibration modes and could be ignored. This study used an acoustic-solid coupling model to separately determine the flow in the impeller water region and the dynamic characteristics of the coupled fluid-solid model. The wet modal analysis of the various length rotors in the sump pump used water as the working medium with the results closer the results of the natural frequency and critical speed of the actual operation of the sump pump rotor [23, 24] is shown in Table 8.

The predicted and measured first-order critical speeds are compared, as shown in Figure 10 which shows little difference between the predictions and the manufacturer data with very similar trends. The differences are mainly due to the limitations of the flow field calculations, especially since the flow model cannot perfectly reproduce all the details of the actual geometry. The first-order critical speed of the rotor gradually decreases as the shaft length increases.

The predicted natural frequencies for the wet mode are compared with those for the dry mode with the prestresses, as shown in Figure 11. The results show that the rotor natural frequencies are lower in the wet mode than in the dry mode for all the shaft lengths with an average decrease of about 16%. When the pump is submerged, the water adds additional weight on the surfaces which affects the dynamics and reduces the natural frequency. Additional calculations showed that changing the water to slurry reduced the natural frequency even more because the slurry is denser than water. Thus, when the sump pump works in slurry, the additional

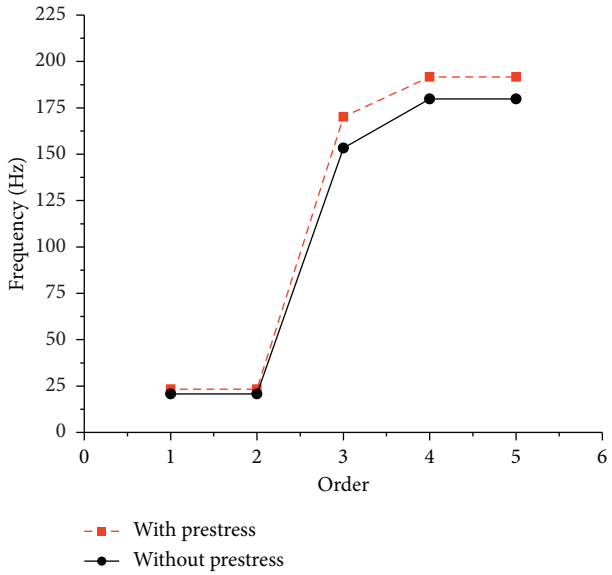

Figure 9: Natural frequencies of the rotor for $D = 1500$.

Table 8: Predicted first natural frequencies and measured [22] and predicted critical speeds for various rotor lengths from the wet mode analysis.

D (mm)	Predicted first natural frequency f (Hz)	Predicted first critical speed n (RPM)	Measured first critical speed [22], n (RPM)
900	48.265	2878	3467
1200	29.194	1741	2107
1500	19.482	1158	1429
1800	14.326	850	1038
2000	11.753	700	862
2400	8.340	498	623
2700	6.711	399	505
3000	5.531	330	417

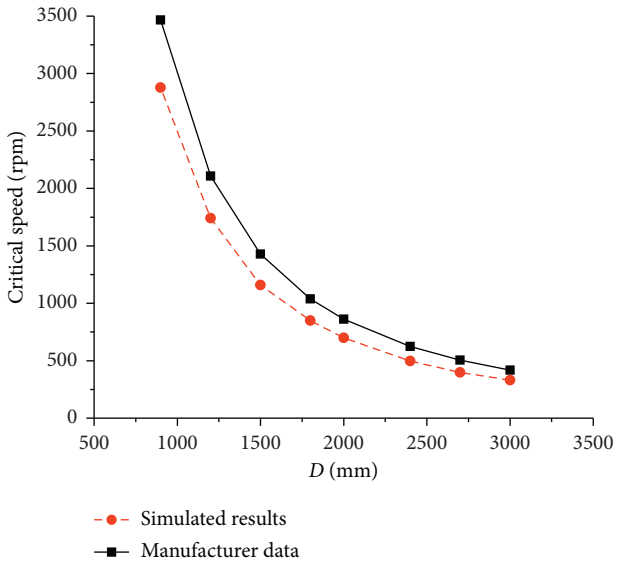

Figure 10: Comparison of the predicted first critical speeds with measured data [22].

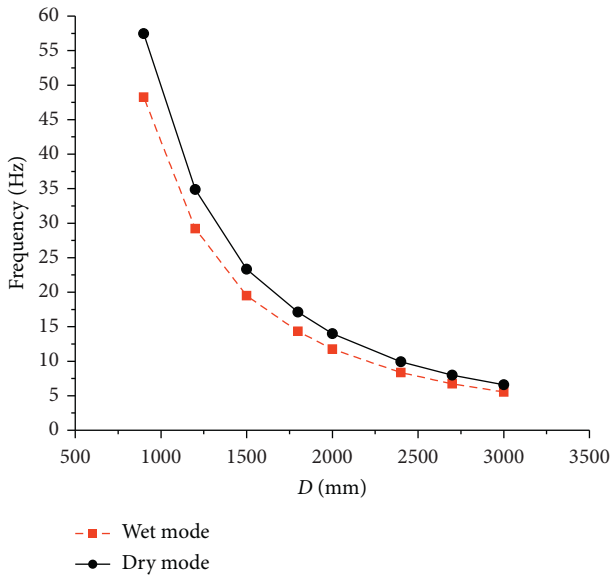

Figure 11: Natural frequencies for the dry and wet modes.

mass of the slurry on the rotor components further reduces the natural frequency. It can be inferred from this that when the structure works in different fluid media [25], due to the different density of the fluid media, the additional mass produced on the surface of the structure will also change, and the mode of the structure will be affected to different degrees.

5. Conclusions

The natural frequencies of various length shafts in a sump pump were analyzed with and without flow in the pump. The results show that the calculations showed that the first-order natural frequency and the critical speed of the sump pump rotor structure decreased with increasing pump shaft length. This trend has been seen in previous manufacturer data. The dry mode analysis showed that application of the fluid forces and other prestresses to the sump pump rotor components resulted in stress stiffening of the components with higher natural frequencies of the rotor components for the various shaft lengths than with no prestresses. The stress stiffening was even more obvious in the higher-order modes. Acoustic-solid coupling was used with a wet modal analysis of the sump pump rotor components with the prestresses. The results show that the natural frequency of the pump rotor components of the wet mode is about 16% less than that in the dry mode because the additional mass of the water on the surfaces reduces the natural frequency of the structure. Thus, changing the fluid medium in the pump, such as using slurries, will change the additional mass on the surfaces due to the different densities which will then affect the pump rotor modal distribution.

Data Availability

The data used to support the findings of this study are included within the article.

Conflicts of Interest

The authors declare that they have no conflicts of interest.

Acknowledgments

This work was supported by the Open Research Fund Program of State Key Laboratory of Hydroscience and Engineering (Grant no. sklhse-2020-E-01).

References

[1] Y. Yang, L. Zhou, W. Shi, Z. He, Y. Han, and Y. Xiao, "Interstage difference of pressure pulsation in a three-stage electrical submersible pump," *Journal of Petroleum Science and Engineering*, vol. 196, Article ID 107653, 2020.

[2] G. Hou, H. Taherian, L. Li, J. Fuse, and L. Moradi, "System performance analysis of a hybrid ground source heat pump with optimal control strategies based on numerical simulations," *Geothermics*, vol. 86, Article ID 101849, 2020.

[3] G. Peng, X. Huang, L. Zhou, G. Zhou, and H. Zhou, "Solid-liquid two-phase flow and wear analysis in a large-scale centrifugal slurry pump," *Engineering Failure Analysis*, vol. 114, Article ID 104602, 2020.

[4] L. Zhou, K. Deshpande, X. Zhang, and R. Agarwal, "Process simulation of Chemical Looping Combustion using ASPEN Plus for a mixture of biomass and coal with various oxygen carriers," *Energy*, vol. 195, Article ID 116955, 2020.

[5] L. Bai, L. Zhou, X. Jiang, Q. Pang, and D. Ye, "Vibration in a multistage centrifugal pump under varied conditions," *Shock and Vibration*, vol. 2019, Article ID 2057031, 9 pages, 2019.

[6] S. Tang, S. Yuan, and Y. Zhu, "Deep learning-based intelligent fault diagnosis methods toward rotating machinery," *Institute of Electrical and Electronics Engineers Access*, vol. 8, no. 1, pp. 9335–9346, 2020.

[7] A. Sukma Nugraha, I. Djunaedi, and H. S. Alam, "Evaluation of critical speed of the rotor generator system based on ANSYS," *Applied Mechanics and Materials*, vol. 799-800, pp. 625–628, 2015.

[8] A. Jameel, A. Abdul Hussein Ali, and T. Mohammad, "Dynamic stability analysis and critical speed of rotor supported by a worn fluid film," *Journal Bearings. Engineering Journal*, vol. 22, no. 3, pp. 148–167, 2016.

[9] S. Tang, S. Yuan, and Y. Zhu, "Convolutional neural network in intelligent fault diagnosis toward rotatory machinery," *Institute of Electrical and Electronics Engineers Access*, vol. 8, no. 1, pp. 86510–86519, 2020.

[10] L. Zhou, W. Shi, W. Lu, B. Hu, and S. Wu, "Numerical investigations and performance experiments of a deep-well centrifugal pump with different diffusers," *ASME Journal of Fluids Engineering*, vol. 134, no. 07, 8 pages, Article ID 0711002, 2012.

[11] Z. Guo, F. Chen, P. Wu, and Z. Qian, "Three-dimensional simulation of air entrainment in a sump pump," *Journal of Hydraulic Engineering*, vol. 143, no. 9, Article ID 4017024, 2017.

[12] I. Park, H. Kim, H. Seong, and D. Rhee, "Experimental studies on surface vortex mitigation using the floating anti-vortex device in sump pumps," *Water*, vol. 10, no. 4, p. 441, 2018.

[13] F. Khan, M. Panchagnula, and K. Velusamy, "Experimental and computational investigations of gas entrainment in SFR due to rotation of partially submerged pump shaft," *Annals of Nuclear Energy*, vol. 143, Article ID 107413, 2020.

[14] Z. Zhang, W. Shi, D. Zhang et al., "Modal analysis of rotor parts of LNG low temperature submersible pump based on thermo-fluid-structure coupling," *Journal of Drainage and Irrigation Machinery Engineering*, vol. 37, no. 3, pp. 211–215, 2019.

[15] Y. Yang, L. Zhou, J. Hang, D. Du, W. Shi, and Z. He, "Energy characteristics and optimal design of diffuser meridian in an electrical submersible pump," *Renewable Energy*, vol. 167, pp. 718–727, 2021.

[16] D. Paule and M. A. Christof, "How shape and flapping rate affect the distribution of fluid forces on flexible hydrofoils," *Journal of Fluid Mechanics*, vol. 901, 2020.

[17] H. Ren, M. Zhang, Y. Wang, Y. Xu, and B. Zhao, "Drag and added mass coefficients of a flexible pipe undergoing vortex-induced vibration in an oscillatory flow," *Ocean Engineering*, vol. 210, Article ID 107541, 2020.

[18] X. Jiang, L. Wang, L. Zhou, W. Li, and C. Wang, "Transient response analysis of cantilever multistage centrifugal pump based on multi-source excitation," *Journal of Low Frequency Noise, Vibration and Active Control*, vol. 39, no. 4, pp. 908–924, 2020.

[19] X. Zhang, *Modal Analysis of Car Body in White*, pp. 33–35, Jiangsu University, Zhenjiang, China, 2002.

[20] Q. Li, C. Kang, and Y. Zhu, "Influence of volute structure on rotor operational stability in high-temperature centrifugal molten-salt pump," *Journal of Drainage and Irrigation Machinery Engineering*, vol. 38, no. 1, pp. 15–20, 2020.

[21] L. Zhou, C. Han, L. Bai, W. Li, M. El-Emam, and W. Shi, "CFD-DEM bidirectional coupling simulation and experimental investigation of particle ejections and energy conversion in a spouted bed," *Energy*, vol. 2020, Article ID 118672, 2020.

[22] Warman International Ltd, "Pump performance curves," Report 100E43, Warman International Ltd., Lancashire, OL, USA, 1989.

[23] P. Bonello, "The extraction of Campbell diagrams from the dynamical system representation of a foil-air bearing rotor model," *Mechanical Systems and Signal Processing*, vol. 129, 2019.

[24] H. She, C. Li, Q. Tang, and B. Wen, "Influence mechanism of disk position and flexibility on natural frequencies and critical speeds of a shaft-disk-blade unit," *Journal of Sound and Vibration*, vol. 469, Article ID 115156, 2020.

[25] H. Yan, X. Su, H. Zhang et al., "Design approach and hydrodynamic characteristics of a novel bionic airfoil," *Ocean Engineering*, vol. 216, Article ID 108076, 2020.